MCB
Journals.ASM.org

Myocardial ATGL Overexpression Decreases the Reliance on Fatty Acid Oxidation and Protects against Pressure Overload-Induced Cardiac Dysfunction

Petra C. Kienesberger,[a,b] Thomas Pulinilkunnil,[a,b] Miranda M. Y. Sung,[a,b,c] Jeevan Nagendran,[a,d] Guenter Haemmerle,[e] Erin E. Kershaw,[f] Martin E. Young,[g] Peter E. Light,[h] Gavin Y. Oudit,[i] Rudolf Zechner,[e] and Jason R. B. Dyck[a,b,c]

Cardiovascular Research Centre, Mazankowski Alberta Heart Institute,[a] and Departments of Pediatrics,[b] Pharmacology,[c] and Medicine,[d] Faculty of Medicine and Dentistry, University of Alberta, Edmonton, Alberta, Canada; Institute of Molecular Biosciences, University of Graz, Graz, Austria[e]; Division of Endocrinology and Metabolism, Department of Medicine, University of Pittsburgh, Pittsburgh, Pennsylvania, USA[f]; Department of Medicine, University of Alabama at Birmingham, Birmingham, Alabama, USA[g]; Department of Pharmacology, Alberta Diabetes Institute and Cardiovascular Research Centre, Faculty of Medicine and Dentistry, University of Alberta, Edmonton, Alberta, Canada[h]; and Division of Cardiology, Department of Medicine, Mazankowski Alberta Heart Institute, University of Alberta, Edmonton, Canada[i]

Alterations in myocardial triacylglycerol content have been associated with poor left ventricular function, suggesting that enzymes involved in myocardial triacylglycerol metabolism play an important role in regulating contractile function. Myocardial triacylglycerol catabolism is mediated by adipose triglyceride lipase (ATGL), which is rate limiting for triacylglycerol hydrolysis. To address the influence of triacylglycerol hydrolysis on myocardial energy metabolism and function, we utilized mice with cardiomyocyte-specific ATGL overexpression (MHC-ATGL). Biochemical examination of MHC-ATGL hearts revealed chronically reduced myocardial triacylglycerol content but unchanged levels of long-chain acyl coenzyme A esters, ceramides, and diacylglycerols. Surprisingly, fatty acid oxidation rates were decreased in *ex vivo* perfused working hearts from MHC-ATGL mice, which was compensated by increased rates of glucose oxidation. Interestingly, reduced myocardial triacylglycerol content was associated with moderately enhanced *in vivo* systolic function in MHC-ATGL mice and increased isoproterenol-induced cell shortening of isolated primary cardiomyocytes. Most importantly, MHC-ATGL mice were protected from pressure overload-induced systolic dysfunction and detrimental structural remodeling following transverse aortic constriction. Overall, this study shows that ATGL overexpression is sufficient to alter myocardial energy metabolism and improve cardiac function.

Myocardial triacylglycerol (TG) is stored in cytosolic lipid droplets within cardiomyocytes and constitutes a critical fatty acid (FA) and energy reserve for the heart. Metabolism of cardiac TG is highly dynamic (2, 29), which likely evolved as a means to ensure continuous FA supply for mitochondrial oxidation independent of short-term fluctuations in plasma FA availability. Previous studies have shown that FAs released by intracellular TG hydrolysis contribute significantly to the generation of ATP necessary for contractile function (2, 34, 39), suggesting that TG hydrolysis plays a critical role in regulating cardiac function. In agreement with this finding, dysregulation of myocardial TG metabolism and either increased or reduced TG content have been associated with cardiac dysfunction and/or heart failure induced by obesity, diabetes, aging, ischemia, and hemodynamic pressure overload (3, 5, 8, 22, 26, 31–34). Moreover, a clear correlation between increased myocardial TG content and decreased cardiac function has been established in rodents and humans (7, 12, 22, 24), supporting the concept that excessive TG accumulation in the heart is detrimental. On the other hand, it has also been postulated that increasing TG content and sequestration of potentially lipotoxic FA metabolites in the myocardial TG pool can be beneficial for heart function (28, 42). As such, the physiological consequences of preventing myocardial TG accumulation with regard to normal physiology and disease remain to be elucidated.

As the enzymes that control TG lipolysis may have an as yet underappreciated role in the regulation of cardiac function in both the healthy and the diseased myocardium, we characterized the importance of adipose triglyceride lipase (ATGL) in the heart. ATGL has been identified as the enzyme that catalyzes the initial step of intracellular TG hydrolysis and is the rate-limiting TG lipase in most tissues, including the myocardium (15, 48). In agreement with this, mice with global targeted deletion of ATGL develop severe lipotrophic cardiomyopathy, resulting in premature mortality (15). Similarly, mutations in the gene coding for ATGL in humans (*PNPLA2*) lead to myocardial steatosis, cardiomyopathy, and heart failure (18, 40). The severity of the cardiac phenotype in mice and humans with ATGL inactivation begs the question whether myocardial ATGL regulates cardiac function secondary to changes in TG metabolism. Thus, we hypothesized that enhanced ATGL activity in the heart and chronically decreased myocardial TG content would be beneficial for cardiac function.

To test the effect of a cardiac-specific increase in ATGL expression, we generated cardiomyocyte-specific ATGL-overexpressing (MHC-ATGL) mice and used this mouse model to investigate whether forced expression of ATGL in the cardiomyocyte was sufficient to enhance myocardial TG hydrolysis, decrease the cardiomyocyte TG content, alter myocardial energy metabolism, and influence cardiac function at baseline as well as during pathophysiological stress.

Received 24 October 2011 **Returned for modification** 14 November 2011
Accepted 30 November 2011
Published ahead of print 12 December 2011
Address correspondence to Jason R. B. Dyck, jason.dyck@ualberta.ca.

doi:10.1128/MCB.06470-11

MATERIALS AND METHODS

Mice. MHC-ATGL mice were generated in the laboratory of R. Zechner using the α-myosin heavy chain (αMHC) promoter (GenBank accession no. U71441), which was kindly provided by Jeffrey Robbins (Children's Hospital, Cincinnati, OH [13]) and was fused to the full-length murine *Pnpla2* cDNA as described previously (16). Mice were housed on a 12-h light/12-h dark cycle with *ad libitum* access to chow diet (product number 5001 from Lab Diet, St. Louis, MO, with 13.5% kcal from fat) and water. For all experiments, littermate wild-type (WT) mice were used as controls. All protocols involving mice were approved by the University of Alberta Institutional Animal Care and Use Committee.

Analysis of serum lipids. Concentrations of nonesterified FA and TG in serum were determined with the HR series NEFA-HR(2) colorimetric assay (Wako Chemicals, Richmond, VA) and the 2780-400H Infinity TG reagent (Thermo MA), respectively.

Echocardiography and treadmill stress test. Mice were mildly anesthetized using isoflurane, and transthoracic echocardiography was performed using a Vevo 770 high-resolution imaging system equipped with a 30-MHz transducer (RMV-707B; VisualSonics, Toronto, Canada). A Columbus Instruments (Columbus, OH) motor-driven Eco 3/6 treadmill was used to determine running capacity in mice. Mice were familiarized for 3 days with the treadmill, following which they were forced to participate in a graded exercise protocol by increasing the belt speed from 10 m/min (initial 10 min) to 15 m/min (40 min) and finally 17 m/min until the mice reached a state of exhaustion. Exhaustion was defined as the mouse spending >10 consecutive seconds or >50% of the time on the shock grid despite additional manual stimulation.

TAC. Transverse aortic constriction (TAC) was performed as described previously (14). Male 8- to 9-week-old mice were anesthetized by an intraperitoneal injection (0.1 ml/10 g of body weight) of ketamine and xylazine (80 and 12 mg/ml, respectively), intubated, and connected to a mouse ventilator (MiniVent; Harvard Apparatus, Holliston, MA). Following midline sternotomy, a blunt 27-gauge needle was tied to the aorta between the right brachiocephalic artery and left common carotid arteries using prolene suture. The needle was then removed, and chest and skin were closed. Transstenotic gradient as assessed by pulsed-wave Doppler flow studies confirmed pressure overload with gradients ranging from 50 to 70 mmHg (63.1 ± 2.7 mmHg for WT mice, 61.3 ± 2.7 mmHg for MHC-ATGL mice; values are means ± standard errors of the means [SEM], $n = 6$ to 10 mice, $P = 0.7$). *In vivo* cardiac function was assessed at 5 weeks after TAC or sham surgery by transthoracic echocardiography. Mice were euthanized shortly thereafter. Hearts were rinsed briefly with phosphate-buffered saline, and atria were removed. Ventricles were quickly weighed, and apical sections were taken for paraffin embedding and histology. The remaining ventricle tissue was snap-frozen in liquid nitrogen and stored at −80°C until further processing.

Heart perfusions. Hearts were perfused aerobically in working mode with Krebs-Henseleit buffer containing 0.8 or 1.2 mmol/liter oleate or palmitate prebound to 3% delipidated bovine serum albumin, 5 mmol/liter glucose, and 50 μU/ml insulin as described previously (23). Mice were euthanized in the fed state, and hearts were dissected and subsequently perfused. Preload and afterload pressure were set to 11.5 and 50 mmHg, respectively, unless otherwise stated. Following perfusion, atria were removed and ventricles were snap-frozen in liquid nitrogen and stored at −80°C until further processing. For measurement of FA and glucose oxidation rates, hearts were perfused for 30 min with buffer containing 1.2 mmol/liter [9,10-^{3}H]palmitate and 5 mmol/liter [U-^{14}C]glucose. To assess *ex vivo* heart function under high workload conditions, hearts were perfused for an initial period of 30 min at normal workload followed by a 30-min perfusion at 80 mmHg afterload with buffer containing an additional 300 nmol/liter isoproterenol.

Tissue homogenization and lipid analysis. Frozen hearts and livers were ground using mortar and pestle, and tissue powder was homogenized in ice-cold lysis buffer containing 20 mmol/liter Tris-HCl (pH 7.4), 5 mmol/liter EDTA, 10 mmol/liter $Na_4P_2O_7$, 100 mmol/liter NaF, 1% Nonidet P-40, 2 mmol/liter Na_3VO_4, protease inhibitor (product number P8340, 10 μl/ml; Sigma, St. Louis, MO), and phosphatase inhibitor (number 524628, 20 μg/ml; Calbiochem, EMD Chemicals, Gibbstown, NJ) unless otherwise stated. Homogenates were centrifuged at 1,200 × *g* for 20 min at 4°C, and the supernatants were transferred to fresh tubes. Protein concentration in lysates was determined using the bicinchoninic acid (BCA) protein assay kit (number 23255; Pierce, Thermo Fisher Scientific, Rockford, IL), and serum albumin was employed as the standard (number 23210; Pierce). Lysates were aliquoted and stored at −80°C until further usage for immunoblot analysis or lipid extraction. Lipids were extracted from lysate according to the method of Folch (9). Aliquots of the organic phase were transferred to fresh tubes, and the organic solvent was evaporated under a nitrogen stream. To determine TG content, lipid extracts were resuspended in ice-cold 1% Triton X-100 by brief sonication, and TG concentration was measured using a colorimetric kit assay (number 2780-400H Infinity TG reagent; Thermo Fisher Scientific). Quantification of long-chain acyl coenzyme A (acyl-CoA) species and ceramides was performed by high-performance liquid chromatography (HPLC) as described previously (11, 47), and *sn*-1,2-diacylglycerol content was determined using the diacylglycerol (DG) kinase method (37).

Fatty acid uptake. Hearts were perfused for 30 min with buffer containing 1.2 mmol/liter [1-^{14}C]oleate. Lipids were extracted as specified above and reconstituted in $CHCl_3$ spiked with lipid standards (product number 1787, mono-, di-, triacylglycerol mix; number O3880, sodium oleate; number C79409, cholesteryl stearate; number P3556, L-α-phosphatidylcholine [Sigma]). Lipids were separated on silica gel 60 thin-layer chromatography plates (product number 05719856; Thermo Fisher Scientific) using hexane-diethyl ether-acetic acid (70:29:1 [vol/vol/vol]) as mobile phase. Lipid spots were visualized with iodine vapor, and incorporated radioactivity was measured by liquid scintillation counting. FA uptake was determined as the sum of FA oxidation and incorporation, similar to methods described previously (17, 20, 30).

Immunoblot analysis. Tissue lysates were resolved by SDS-PAGE, and proteins were transferred onto a nylon membrane. Blotted proteins were reversibly visualized using MemCode stain (Pierce) and identified using the primary antibodies: anti-ATGL (product number 2138; Cell Signaling, Beverly, MA), anti-perilipin-5 (number 03-GP31; American Research Products, Belmont, MA), anti-p85PI3K (number 06-497; Millipore, Billerica, MA), anti-SERCA (ATP2A2, number 4388; Cell Signaling), anti-phospho(Ser16)PLN (number 07-052, Millipore); anti-phospho(Thr17)PLN (number sc-17024-R; Santa Cruz, Biotechnology, Santa Cruz, CA), anti-PLN (number NB300-582; Novus Biologicals, Littleton, CO), anti-phospho(Tyr705)STAT3 (number 9131; Cell Signaling), anti-STAT3 (number sc-8019; Santa Cruz), anti-OXPHOS (number 604; MitoSciences/Abcam, Cambridge, United Kingdom), and anti-CD36/FAT (number NB400-144H; Novus Biologicals) antibodies. Immunoblots were developed using the Western Lightning Plus-ECL enhanced chemiluminescence substrate (Perkin Elmer, Waltham, MA). Densitometric analysis was performed using ImageJ software (National Institutes of Health, Bethesda, MD) or Carestream Molecular Imaging software (Rochester, NY).

Triacylglycerol hydrolase activity. Frozen ventricular tissue was homogenized in ice-cold lysis buffer containing 0.25 mol/liter sucrose, 1 mmol/liter EDTA, 1 mmol/liter dithiothreitol, 20 μg/ml leupeptin, 2 μg/ml antipain, and 1 μg/ml pepstatin (pH 7.0) and spun at 20,000 × *g* for 30 min at 4°C. The infranatant (100 μg of protein in 100 μl lysis buffer) was incubated with 100 μl of substrate in a water bath for 60 min at 37°C. The reaction was terminated by the addition of 3.25 ml of methanol-chloroform-heptane (10:9:7 [vol/vol/vol]) and 1 ml of 0.1 mol/liter potassium carbonate–0.1 mol/liter boric acid, pH 10.5, and samples were vigorously mixed for extraction. After centrifugation (800 × *g*, 20 min), radioactivity in 1 ml of the upper phase was determined by liquid scintillation counting. TG substrate contained 33 nmol of glycerol trioleate/assay (glycerol tri[9,10(n)-^{3}H]oleate 40,000 cpm/nmol) in 50 mmol/liter

potassium phosphate buffer, pH 7.0, and 2.5% defatted bovine serum albumin and was prepared by sonication on ice.

Isolated ventricular cardiomyocyte studies. Ventricular cardiomyocytes were isolated as described previously (19). For cell shortening studies, freshly isolated cardiomyocytes were continuously superfused at 1 ml min^{-1} with Krebs-Henseleit buffer containing 2 mmol/liter Ca^{2+} and electrically paced at 1 Hz by field stimulation. Single myocyte contractility was measured using a video edge detector (Crescent Electronics, Salt Lake City, UT), and data were recorded and analyzed using pClamp 8.0 software. Cell shortening was expressed as percentage of fractional shortening, i.e., [(resting myocyte length − contracted myocyte length)/resting myocyte length] × 100. Experiments were performed at 21°C. For measurement of calcium transients, isolated myocytes were loaded with 10 μmol/liter Fluo-4 AM (Invitrogen, Carlsbad, CA) for 30 min at 21°C. Following removal of excess dye, single myocyte calcium transients were measured using a photomultiplier tube detection system, and data were recorded and analyzed using pClamp 10.0 software.

Gene expression. Gene expression analysis was performed by quantitative reverse transcriptase PCR as previously described (45). The following primer and probe sequences were used for quantitative PCR analysis (FAM is 6-carboxyfluorescein and TAMRA is 6-carboxytetramethylrhodamine): *Pnpla2* forward, 5′-GGTCCTCCGAGAGATGTGC-3′; *Pnpla2* reverse, 5′-TGGTTCAGTAGGCCATTCCTC-3′; *Pnpla2* probe, 5′-FAM-CAGGGCTACAGAGATGGACTTCGATTCCTT-TAMRA-3′; *Cte1* forward, 5′-ACCCCCTGTGACTATCCTGAG-3′; *Cte1* reverse, 5′-TTCTAC CAGAGGGCTTTGCA-3′; *Cte1* probe, 5′-FAM-AGCATCTACAACATC CTTGAGGCCATCCT-TAMRA-3′; *UCP3* forward, 5′-TGCTGAGATG GTGACCTACGA-3′; *UCP3* reverse, 5′-CCAAAGGCAGAGACAAAGT GA-3′; *UCP3* probe, 5′-FAM-AAGTTGTCAGTAAACAGGTGAGACTC CAGCAA-TAMRA-3′; *Pdk4* forward, 5′-TTCACACCTTCACCACATG C-3′; *Pdk4* reverse, 5′-AAAGGGCGGTTTTCTTGATG-3′; *Pdk4* probe, 5′-FAM-CGTGGCCCTCATGGCATTCTTG-TAMRA-3′; *Mcd* forward, 5′-CGGCACCTTCCTCATAAAGC-3′; *Mcd* reverse, 5′-GGGTAT AGGTGACAGGCTGGA-3′; *Mcd* probe, 5′-FAM-AGTGGTCAAGGAG CTGCAGAAGGAGTTT-TAMRA-3′; *Pgc1α* forward, 5′-AGAAGCGGG AGTCTGAAAGG-3′; *Pgc1α* reverse, 5′-CAGTTCTGTCCGCGTTGTG-3′; *Pgc1α* probe, 5′-FAM-AGAAAGCAATTGAAGAGCGCCGTGTG-TAMRA-3′; *Mcad* forward, 5′-TGGCATATGGGTGTACAGGG-3′; *Mcad* reverse, 5′-CCAAATACTTCTTCTTCTGTTGATCA-3′; *Mcad* probe, 5′-FAM-AGGCATTTGCCCCAAAGAATTTGCTTC-TAMRA-3′; *Lcad* forward, 5′-GGAGTAAGAACGAACGCCAA-3′; *Lcad* reverse, 5′-GCCA CGACGATCACGAGAT-3′; *Lcad* probe, 5′-FAM-CCATTAITGATGAA CACCTTGCTTCCATTGA-TAMRA-3′; *Accβ* forward, 5′-ACTTTGACC TGACCGCTGTG-3′; *Accβ* reverse, 5′-CTGAGTGCCGGATAATGGC-3′; *Accβ* probe, 5′-FAM-TGCATCTTTACCTGGGAGCCGCTAAG-TAMRA-3′; *Agpat3* forward, 5′-TGGAAGACATCCCAGCAGAT-3′; *Agpat3* reverse, 5′-CCCCTGGGAATACACCCTT-3′; *Agpat3* probe, 5′-FAM-AGGAGAAGGATGCCCTGCAAGAGATGTA-TAMRA-3′; *Dgat2* forward, 5′-GGCTGGCATTTGACTGGAA-3′; *Dgat2* reverse, 5′-TGGT CAGCAGGTTGTGTGTCT-3′; *Dgat2* probe, 5′-FAM-AAGAAAGGTGG CAGGAGATCGCAGTG-TAMRA-3′; *Nppa* forward, 5′-TGGAAGACA TCCCAGCAGAT-3′; *Nppa* reverse, 5′-CCCCTGGGAATACACCCTT-3′; *Nppa* probe, 5′-FAM-AGGAGAAGGATGCCCTGCAAGAGATGTA-TAMRA-3′; *Nppb* forward, 5′-CAGAAGCTGCTGGAGCTGA-3′; *Nppb* reverse, 5′-AGGGCCTTGGTCCTTTGAG-3′; *Nppb* probe, 5′-FAM-AG AGAAAAGTCAGAGGAAATGGCTCAGAGACA-TAMRA-3′; *Myh7* forward, 5′-GATGTTTTTGTGCCCGATGA-3′; *Myh7* reverse, 5′-TGTC GAACTTGGGTGGGTT-3′; *Myh7* probe, 5′-FAM-CAGTCACCGTCTT GCCATTCTCCGT-TAMRA-3′.

Nucleotide measurement. Hearts were perfused for 60 min with buffer containing 0.8 mmol/liter oleate, and nucleotides were extracted from 20 to 30 mg of frozen ventricular tissue by homogenization in ice-cold 6% (vol/vol) perchloric acid-1 mmol/liter dithiothreitol-0.5 mmol/liter EGTA. Homogenates were spun at 12,000 × *g* for 5 min at 4°C, and pH in supernatants was neutralized using K_2CO_3. Samples were kept on ice for an additional 30 min, followed by centrifugation at 10,000 × *g* for 2 min at 4°C. Nucleotide concentrations in supernatants were determined by HPLC.

Histology. Hematoxylin and eosin and Masson's trichrome stains of paraffin-embedded sections were visualized using a Leica DMLA microscope (Leica Microsystems, Wetzlar, Germany) equipped with a Retiga 1300i FAST 1394 CCD camera (QImaging, Surrey, BC, Canada). Cardiomyocyte cross-sectional areas were analyzed using ImageJ software.

Statistical analysis. Results are expressed as means ± SEM. Statistical analyses were performed using SigmaPlot and GraphPad Prism software. Comparisons between two groups were made by unpaired two-tailed Student's *t* test. For comparisons between more than two groups, one-way analysis of variance (ANOVA) followed by Newman-Keuls multiple comparison test was utilized. *P* values of less than 0.05 were considered statistically significant.

RESULTS

Myocardial TG content is chronically reduced in MHC-ATGL mice. Hearts from MHC-ATGL mice showed a significant increase in both *Pnpla2* (*Atgl*) mRNA levels (Fig. 1A) and ATGL protein expression (Fig. 1B). Overexpression of ATGL was myocardium specific, as ATGL protein expression in other tissues, such as skeletal muscle, was unchanged (Fig. 1B). This significant increase in ATGL expression resulted in a more moderate 5.7-fold increase in TG hydrolase activity in the myocardium of MHC-ATGL mice compared to WT controls (Fig. 1C), which corresponded with a significant reduction of TG content in hearts from MHC-ATGL mice compared to WT mice in fed and fasted states (Fig. 1D). In addition, fasting induced an increase in myocardial TG content in the WT but not in MHC-ATGL mice (Fig. 1D). Cardiac TG content was also reduced in MHC-ATGL hearts compared to WT hearts following aerobic perfusion in the working mode *ex vivo* (Fig. 1E). Serum FA and TG levels were similar between genotypes (FA levels after 4 h of fasting, 0.77 ± 0.08 μmol/liter for WT, 0.78 ± 0.03 μmol/liter for MHC-ATGL, $P = 0.9$; TG levels after 4 h of fasting, 56.80 ± 3.58 mg/dl for WT, 55.01 ± 6.05 mg/dl for MHC-ATGL, $P = 0.8$; values are means ± SEM, $n = 7$ mice, 11- to 13-week-old males), demonstrating that cardiac-specific ATGL overexpression does not affect plasma lipid levels. Consistent with lower myocardial TG content, MHC-ATGL mice also displayed reduced cardiac expression of the cardiomyocyte lipid droplet protein, perilipin-5 (PLIN5; also known as OXPAT) (Fig. 1B). Interestingly, despite the chronic reduction in TG content, hearts from MHC-ATGL mice had unchanged levels of DG (Fig. 1F), ceramides (Fig. 1G), and long-chain acyl-CoAs (Fig. 1H). In addition, histological analysis of ventricular sections stained with hematoxylin and eosin or Masson's trichrome stain showed no evidence of abnormal cardiomyocyte morphology or collagen deposition (Fig. 1I).

Systolic heart function is moderately improved in MHC-ATGL mice. To determine the functional consequences of ATGL overexpression under normal physiologic conditions *in vivo*, we performed transthoracic echocardiography on mildly anesthetized mice at 31 to 33 weeks of age (body weight, 29.0 ± 0.2 g for WT, 28.1 ± 0.4 g for MHC-ATGL, $P = 0.5$; values are means ± SEM, $n = 6$ mice). Since anesthesia suppresses heart rate and cardiac contractility, isoflurane dosage was adjusted such that heart rates were comparable between genotypes (453 ± 6 beats per minute [bpm] for WT, 482 ± 9 bpm for MHC-ATGL, $P = 0.3$; values are means ± SEM, $n = 6$ mice). Ejection fraction and velocity of circumferential fiber shortening were increased by 9 and 22%, respectively, in MHC-ATGL mice compared to WT mice

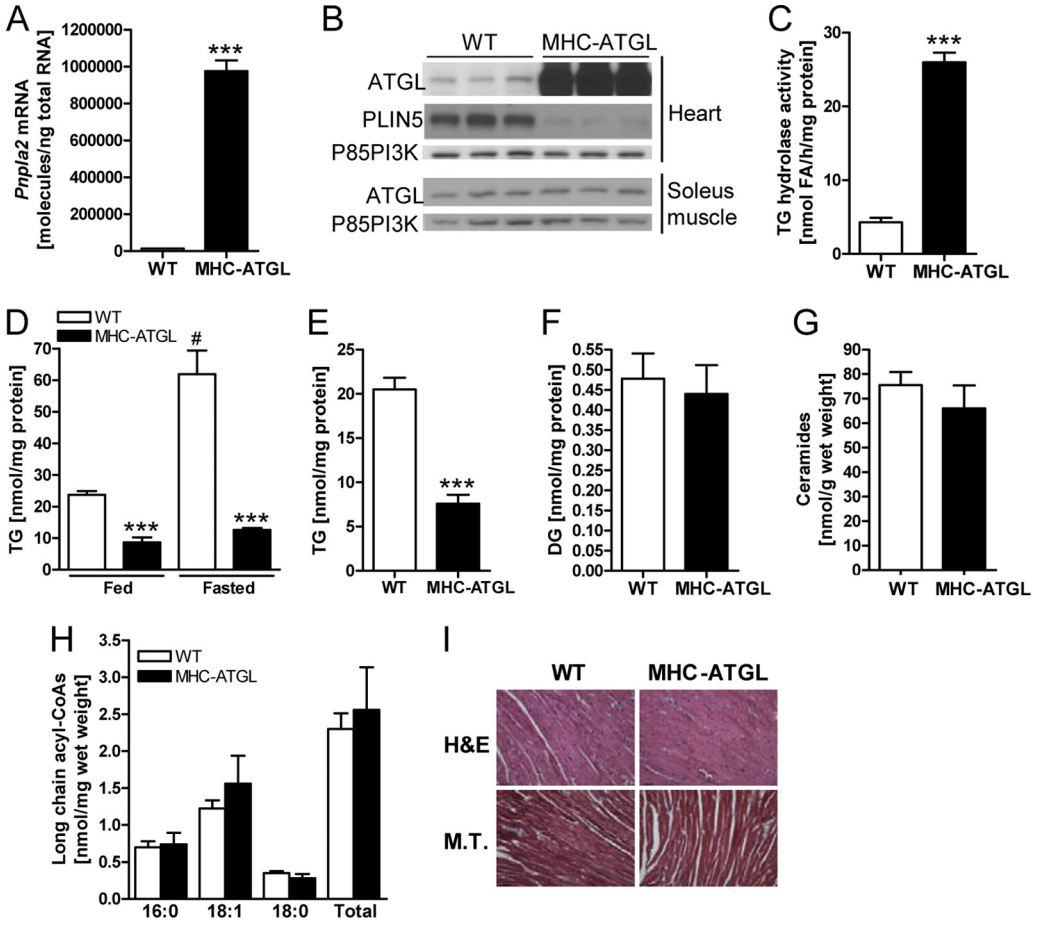

FIG 1 Biochemical and histological characterization of WT and MHC-ATGL hearts. (A) Cardiac *Pnpla2* (*Atgl*) mRNA expression in 4- to 5-h-fasted male mice (11 to 13 weeks old, $n = 7$; ***, $P < 1 \times 10^{-8}$). (B) Immunoblots showing ATGL protein expression in the heart and soleus muscle as well as PLIN5 expression in the heart from 4- to 5-h-fasted male mice (35 to 36 weeks old). The p85 subunit of PI3K (p85PI3K) served as the loading control. (C) Cytoplasmic TG hydrolase activity in heart homogenates from fed mice (mixed gender, 15 weeks old, $n = 4$; ***, $P < 0.0001$). (D) Myocardial TG content in fed and 16-h-fasted mice (mixed gender, 13 to 25 weeks old, $n = 7$ or 8 for fed, $n = 3$ for fasted; ***, $P < 0.001$ versus WT; #, $P < 0.001$ versus fed). (E) TG content in isolated *ex vivo* perfused working hearts from male mice (18 weeks old, $n = 6$ to 8; ***, $P < 0.0001$). Hearts were perfused for 60 min with 0.8 mmol/liter oleate and 5 mmol/liter glucose in the presence of 50 μU/ml insulin. (F) DG content in hearts from 5-h-fasted female mice (20 to 21 weeks old, $n = 4$ or 5). Myocardial ceramide content (G) and long-chain acyl-CoA content (H) of male 4- to 5-h-fasted mice (35 to 36 weeks old, $n = 5$). (I) Representative histological images of apical heart sections stained with hematoxylin and eosin (H&E) and Masson's trichrome (M.T.) stain at ×400 magnification. Scale bars indicate 30 μm.

(Fig. 2A to C). This modest improvement in contractile function in MHC-ATGL hearts was associated with decreased left ventricular internal diameters during diastole (LVIDd) and, to a greater extent, during systole (LVIDs) (Fig. 2D and E). Parameters of diastolic function, such as mitral E/A (ratio of early [E] to late [A] ventricular filling velocity), isovolumic relaxation time, and mitral valve deceleration time were comparable between genotypes (data not shown). These data, which are representative of three independent cohorts of mice 31 to 34 weeks old, suggest that ATGL overexpression leads to a moderately improved systolic function *in vivo* without changes in diastolic function. The thickness of the interventricular septum (IVS) and left ventricular posterior wall (LVPW) was also slightly increased in MHC-ATGL hearts compared to WT hearts (Fig. 2F and G). However, the ratio of ventricle weight to tibia length was unchanged (Fig. 2H), suggesting the absence of overt hypertrophy in MHC-ATGL hearts.

Next we examined whether ATGL overexpression could improve the contractility of isolated primary cardiomyocytes in cell shortening studies. Indeed, while cell shortening of adult mouse cardiomyocytes, determined as percent change in cell length upon contraction, in the absence of isoproterenol was similar between genotypes (Fig. 3A), the increase in cell shortening was significantly greater in ATGL-overexpressing cardiomyocytes than in WT cardiomyocytes when stimulated with isoproterenol (Fig. 3B). To test whether increased calcium cycling could underlie the enhanced contractility in MHC-ATGL cardiomyocytes, we measured calcium transients in isolated primary cardiomyocytes and analyzed expression and phosphorylation of proteins involved in cardiomyocyte calcium handling. We found that the isoproterenol-induced increases in calcium transients were similar between cardiomyocytes from WT and MHC-ATGL mice (Fig. 3C). In addition, cardiac protein expressions of sarco/endoplasmic reticulum Ca^{2+}-ATPase (SERCA) as well as phosphorylation of phospholamban (PLN) were comparable between genotypes (Fig. 3D), suggesting that calcium cycling in MHC-ATGL cardiomyocytes is unaltered.

Hearts from MHC-ATGL mice show enhanced performance when challenged with high workload. Since our previous data

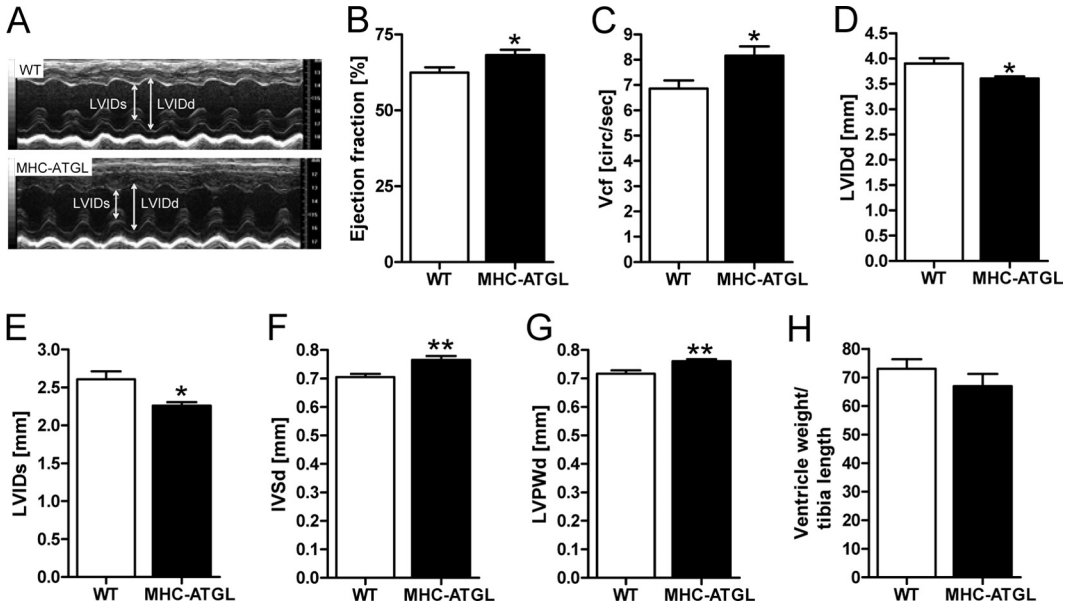

FIG 2 Baseline *in vivo* cardiac function in WT and MHC-ATGL mice. (A to G) Functional parameters obtained by transthoracic echocardiography in male mice (31 to 33 weeks old, $n = 6$; *, $P < 0.05$; **, $P < 0.01$). (A) Representative M-mode images; (B) ejection fraction; (C) velocity of circumferential fiber shortening (Vcf); left ventricular internal diameter in diastole (LVIDd) (D) and in systole (LVIDs) (E); (F) interventricular septal thickness in diastole (IVSd); (G) left ventricular posterior wall thickness in diastole (LVPWd); (H) ratio of heart ventricle weight to tibia length in male mice (35 to 36 weeks old, $n = 5$).

suggested enhanced systolic function in MHC-ATGL hearts, we tested whether these hearts would perform better than WT hearts when challenged with higher workloads. To indirectly test myocardial performance under high workload *in vivo*, we performed a treadmill exercise test where mice were exercised until exhaustion. In this experiment, MHC-ATGL mice ran 20% longer than the WT (Fig. 4A), suggesting that improved performance of MHC-ATGL hearts allowed for the significant increase in exercise capacity. Using *ex vivo* work jump perfusions, during which a 30-min perfusion at normal workload (50 mmHg afterload) was followed by a 30-min period of high workload (80 mmHg afterload, 300 nmol/liter isoproterenol in perfusion buffer), we directly assessed cardiac performance. Heart rates were similar between genotypes at normal workload and increased to a similar extent in WT and MHC-ATGL hearts upon switching to high workload (Fig. 4B). Following 30 min of perfusion at high workload, only 20% of WT hearts were able to produce high enough peak systolic pressure (PSP) to meet the elevated afterload and produce aortic outflow. Conversely, 75% of the hearts from MHC-ATGL mice were able to produce aortic outflow against the increased afterload pressure through increasing PSP above 80 mmHg (Fig. 4C). Together, these findings suggest that improved contractile function of the ATGL-overexpressing hearts allows them to better adapt to elevated workloads.

FA oxidation is decreased and glucose oxidation is increased in hearts from MHC-ATGL mice. To assess whether changes in myocardial energy metabolism could contribute to the increase in systolic function in MHC-ATGL mice, hearts from WT and MHC-ATGL mice were subjected to *ex vivo* perfusions in the working mode using radiolabeled substrates. Since cardiac power *ex vivo* was comparable between genotypes (Fig. 5A), differences in substrate metabolism could be evaluated in the absence of alterations in energetic demand. Interestingly, rates of FA oxidation (FAO) were decreased by 28% in MHC-ATGL hearts (Fig. 5B), and glucose oxidation rates were correspondingly increased by 47% (Fig. 5C) in MHC-ATGL hearts compared to WT hearts. This change in substrate metabolism was observed in hearts from both male and female MHC-ATGL mice and with either palmitate or oleate in the perfusion buffer (data not shown). While there was a shift in the reliance on glucose and FA oxidation for Krebs cycle acetyl-CoA production in MHC-ATGL hearts (Fig. 5D), the absolute production of acetyl-CoA derived from FA and glucose oxidation rates remained comparable between genotypes (data not shown), suggesting no impairment in ATP supply. Consistent with preserved myocardial energetics, cardiac ATP content, ATP-to-AMP ratio, and phosphocreatine-to-ATP ratio were also unchanged in MHC-ATGL hearts (Fig. 5E to G). FA uptake was significantly reduced in MHC-ATGL hearts compared to that observed in WT hearts (Fig. 5H) and was reflected not only by the decrease in FA oxidation but also a 57% decline in FA incorporation into TG (293 ± 47 nmol/g [dry weight]/min for WT, 125 ± 17 nmol/g [dry weight]/min for MHC-ATGL; values are means ± SEM, $P < 0.05$, $n = 4$ mice). Incorporation of FA into other neutral lipids, free FA, and phospholipids was similar between WT and MHC-ATGL hearts (109 ± 10 nmol/g [dry weight]/min for WT, 109 ± 9 nmol/g [dry weight]/min for MHC-ATGL; values are means ± SEM, $P = 0.97$, $n = 4$ mice). Interestingly, the reduction in myocardial FA uptake corresponded with decreased protein expression of the FA translocase, CD36/FAT, in hearts from MHC-ATGL mice (Fig. 5I), further supporting the reduction in FA uptake in hearts from MHC-ATGL mice.

In agreement with reduced FAO in MHC-ATGL hearts, there was decreased mRNA expression of the peroxisome proliferator-activated receptor α/δ (PPARα/δ) target genes, acyl-CoA thioesterase 1 gene (*Cte1*), uncoupling protein 3 gene (*Ucp3*), pyruvate dehydrogenase kinase isozyme 4 gene (*Pdk4*), malonyl-CoA decar-

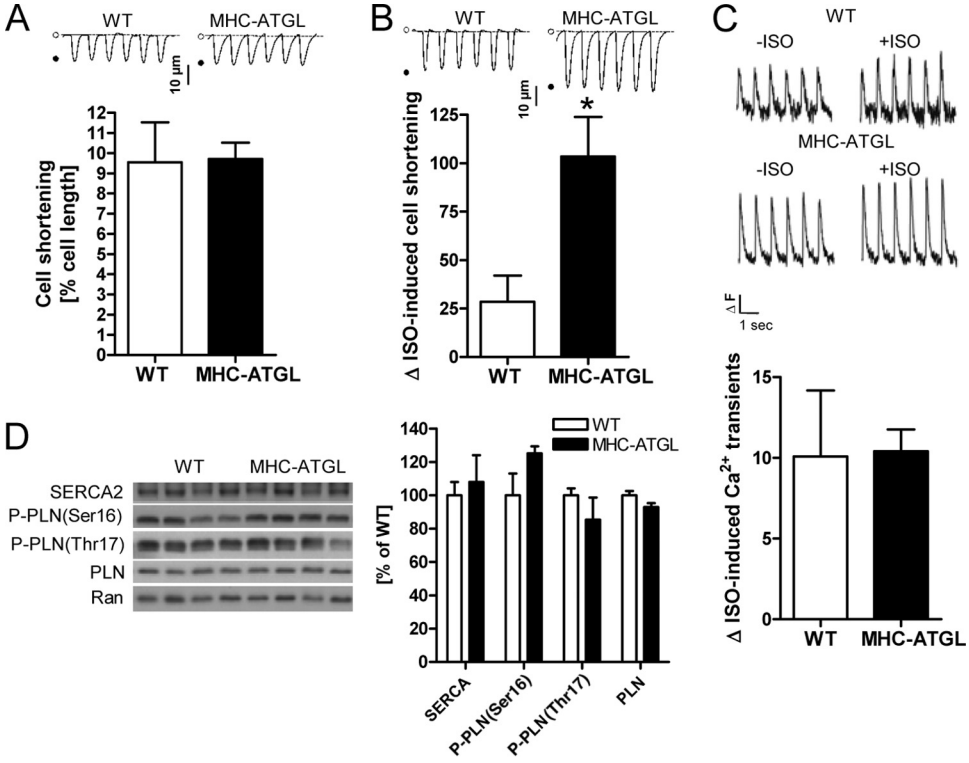

FIG 3 Analysis of cardiomyocyte shortening and calcium homeostasis. (A and B) Cell shortening of isolated cardiomyocytes from female mice (21 to 26 weeks old, $n = 8$ to 13 cardiomyocytes from 3 mice per genotype). Cell shortening in the absence of isoproterenol (A) and percent increase in cell shortening when comparing stimulation with 100 nmol/liter isoproterenol to incubation without isoproterenol (B) (*, $P < 0.05$); insets show representative tracings of cell shortening. (C) Percent increase in calcium transients when comparing stimulation with 100 nmol/liter isoproterenol (+ISO) to incubation without isoproterenol (−ISO) ($n = 7$ or 8 cardiomyocytes from 2 female mice per genotype, 36 to 41 weeks old); insets show representative calcium tracings (ΔF, change in fluorescence intensity). (D) Immunoblots and densitometric analysis showing protein expression of SERCA2 and phospholamban (PLN) as well as phospholamban phosphorylation (P-PLN; ratio of phosphorylated PLN to total PLN) in hearts from male 4- to 5-h-fasted mice (35 to 36 weeks old). Ran GTPase served as the loading control.

boxylase gene (*Mcd*), and acetyl-CoA carboxylase β gene (*Acc*β) in MHC-ATGL hearts (Fig. 5J). PPARγ coactivator 1α (*Pgc1*α) mRNA expression was also reduced in MHC-ATGL hearts compared to WT hearts, while transcript levels of medium- and long-chain acyl-CoA dehydrogenase (*Mcad* and *Lcad*, respectively) were unchanged (Fig. 5J). In addition, expression of the 1-acylglycerol-3-phosphate *O*-acyltransferase 3 gene (*Agpat3*) trended lower, and mRNA levels of diacylglycerol *O*-acyltransferase 2 (*Dgat2*), which is involved in TG synthesis, were decreased in MHC-ATGL hearts compared to WT hearts (Fig. 5J). Protein expressions of subunits from mitochondrial oxidative phosphorylation (OXPHOS) complexes I to V were similar between genotypes (Fig. 5K), suggesting that alterations in OXPHOS abundance are unlikely to contribute to the reduction in FAO in MHC-ATGL hearts. We also examined

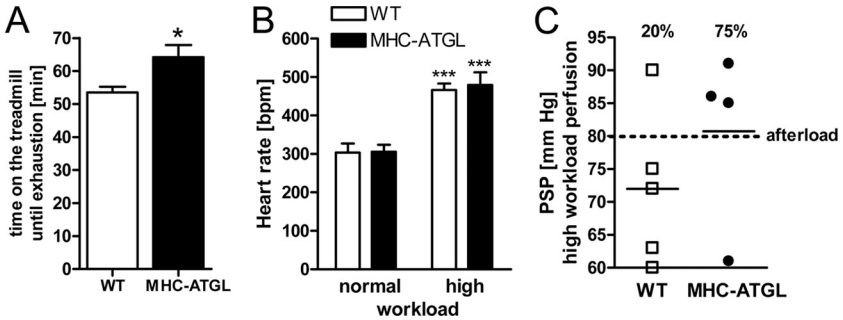

FIG 4 Treadmill test and *ex vivo* work jump perfusion. (A) Maximum run time during treadmill stress test (10- to 12-week-old males, $n = 5$ or 6 mice; *, $P < 0.05$). (B and C) Hearts from female mice (13 to 15 weeks old, $n = 4$ or 5) were perfused in the working mode with 1.2 mmol/liter oleate, 5 mmol/liter glucose, and 50 μU/ml insulin for 30 min at 50 mmHg afterload pressure (normal workload). Subsequently, hearts were perfused with an increased afterload of 80 mmHg and perfusate containing isoproterenol (300 nmol/liter) for an additional 30 min (high workload). (B) Heart rate during normal and high workload perfusion (***, $P < 0.001$ versus normal workload); (C) peak systolic pressure (PSP) at the end of the high workload perfusion. The percentage of hearts that produced aortic outflow until the end of perfusion is indicated.

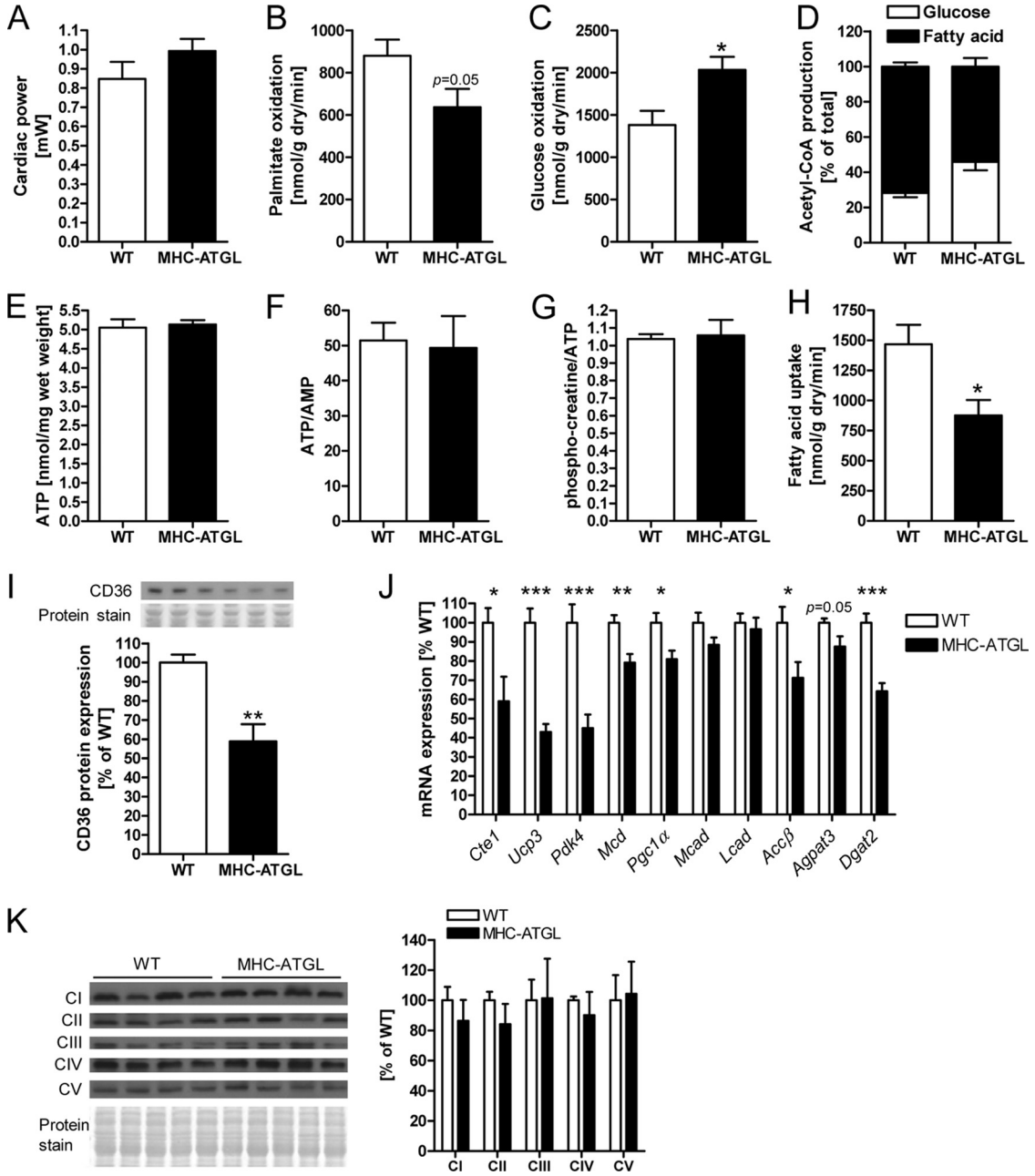

FIG 5 FA and glucose metabolism in WT and MHC-ATGL hearts. (A) Cardiac power; (B) palmitate oxidation rates; (C) glucose oxidation rates; (D) Krebs cycle acetyl-CoA production in *ex vivo* perfused hearts from male 33- to 35-week-old mice ($n = 8$; *, $P < 0.05$); (E) ATP content; (F) ATP-to-AMP ratio; (G) phosphocreatine-to-ATP ratio in *ex vivo* perfused hearts from male mice (17 to 18 weeks old, $n = 5$ to 8); (H) FA uptake in *ex vivo* perfused hearts from female mice (22 to 28 weeks old, $n = 4$; *, $P < 0.05$); (I) myocardial CD36 protein expression in male mice (13 to 16 weeks old, $n = 5$; **, $P < 0.01$); (J) myocardial mRNA expression of genes involved in FA metabolism (4- to 5-h-fasted, 11- to 13-week-old male mice, $n = 7$; *, $P < 0.05$; **, $P < 0.01$; ***, $P < 0.001$); (K) immunoblots and densitometric analysis of myocardial OXPHOS protein expression (4- to 5-h-fasted, 35- to 36-week-old male mice, $n = 5$).

whether the decrease in myocardial FA utilization in MHC-ATGL mice would lead to a redistribution of FA to increase liver TG content. As expected, liver TG content was not elevated in MHC-ATGL mice compared to WT mice but was instead moderately decreased in MHC-ATGL mice (57.9 ± 2.6 nmol/mg protein for WT, 47.3 ± 2.9 nmol/mg protein for MHC-ATGL; values are means ± SEM, $P < 0.05$, $n = 7$ mice, 11- to 13-week-old 4-h-fasted males).

Contractile function is preserved in hearts from MHC-ATGL mice following pressure overload. Since *in vivo* and *ex vivo* studies showed that cardiomyocyte-specific ATGL overexpression improves myocardial performance of a healthy heart, we hypothesized that cardiomyocyte-specific ATGL overexpression would also help to maintain cardiac function when hearts were challenged with increased afterload *in vivo*. To test this hypothesis, WT and MHC-ATGL mice were subjected to transverse aortic con-

striction to provoke pressure overload-induced cardiac hypertrophy and systolic dysfunction. As expected, 5 weeks of TAC produced significant cardiac hypertrophy in WT mice, as evidenced from the increase in the ratio of ventricle weight to tibia length (Fig. 6A), cardiomyocyte cross-sectional area (Fig. 6B and C), and ventricular wall thickness (Fig. 6D) compared to the sham-operated control mice. mRNA expression of the hypertrophy marker genes, the atrial natriuretic peptide (*Nppa*), brain natriuretic peptide (*Nppb*), and myosin heavy chain beta isoform (*Myh7*) genes, and phosphorylation of signal transducer and activator of transcription 3 (STAT3) were also increased in WT hearts subjected to TAC (Fig. 6J and L). While these same measures of cardiac hypertrophy were also increased in MHC-ATGL hearts subjected to TAC, this increase tended to be less pronounced compared to that in WT hearts, especially in the case of the transcriptional expression of the prohypertrophic markers and STAT3 phosphorylation (Fig. 6J and L).

Most importantly and consistent with our previous observations of enhanced performance of MHC-ATGL hearts under high workload, cardiomyocyte-specific ATGL overexpression protected hearts from systolic dysfunction following TAC. Hearts from WT mice had reduced ejection fraction (Fig. 6G) at 5 weeks following TAC compared to the sham controls. In addition, WT hearts presented with marked left ventricle dilation following TAC, as LVID in both systole (Fig. 6H) and diastole (Fig. 6I) were significantly increased compared to the sham-operated WT mice. Remarkably, ejection fractions (Fig. 6G) and LVID (Fig. 6H and I) were similar in hearts from MHC-ATGL mice following TAC and sham surgery. Heart rates during echocardiography were comparable between all groups (Fig. 6F). Together, these data show that ATGL overexpression leads to preserved cardiac function and the prevention of ventricle dilation following TAC. The sustained cardiac function in MHC-ATGL mice following TAC was paralleled by significantly reduced myocardial TG content in MHC-ATGL mice compared to WT mice (Fig. 6K). In addition, the systolic dysfunction in the WT hearts following TAC was associated with a reduction in PLN phosphorylation at Ser16, which was not observed in MHC-ATGL hearts (Fig. 6M). Unlike our previous observations in older (31- to 33-week-old) mice (Fig. 2A to G), ventricle wall thickness, ejection fraction, LVIDs, and LVIDd were not significantly different when comparing the significantly younger (13- to 14-week-old) sham-operated MHC-ATGL to WT mice (Fig. 6D and G to I), suggesting that the increase in baseline systolic function *in vivo* and ventricle wall thickness in MHC-ATGL mice develops with progressing age. We utilized young, 8- to 9-week-old mice for TAC to follow a previously established procedure (14, 21, 36).

DISCUSSION

To date, the role that the enzymes involved in myocardial TG hydrolysis play in regulating cardiac function under physiological and pathological conditions is unclear. As such, we investigated whether cardiomyocyte-specific overexpression of ATGL and the resulting decrease in intramyocardial TG content could influence contractile function.

One of the most remarkable findings of this study is that forced expression of ATGL specifically in cardiomyocytes is able to modestly but significantly improve left ventricular systolic function beyond that observed in a healthy heart. In accordance with moderately increased systolic function *in vivo*, cardiomyocyte-specific ATGL overexpression also prevented a decline in left ventricle function and ventricular dilation when mice were subjected to 5 weeks of TAC-induced pressure overload. Together, these data demonstrate that increased ATGL influences cardiac function at baseline as well as offers protection from pathological cardiac remodeling in response to severe pressure overload. While this improvement in cardiac function was clear in multiple cohorts of mice, there appeared to be an age-dependent effect, as younger mice (13 to 14 weeks of age) did not display this improved function. The mechanisms contributing to this age-induced improvement in cardiac function have not been clearly established.

We examined whether alterations in cardiomyocyte calcium handling could contribute to the increased systolic function in MHC-ATGL hearts. Interestingly, calcium transients in isolated primary cardiomyocytes were similar between genotypes. In accordance with this finding, SERCA2 expression and PLN phosphorylation were unchanged in MHC-ATGL hearts, suggesting that alterations in cardiomyocyte calcium homeostasis are unlikely to contribute to the moderately increased systolic function in MHC-ATGL hearts at baseline. However, it is conceivable that myofilament sensitivity to calcium is increased in MHC-ATGL hearts, leading to enhanced cardiac contractility. We found that TAC-induced pressure overload led to a decline in PLN Ser16 phosphorylation in WT hearts, which was associated with systolic dysfunction and was not observed in ATGL-overexpressing hearts. Based on this finding, we suggest that preserved PLN Ser16 phosphorylation may contribute to the protection against systolic dysfunction in MHC-ATGL hearts following pressure overload.

Next we determined whether altered substrate metabolism and cardiac energetics could underlie the increased systolic function in MHC-ATGL hearts. Interestingly, FAO rates were reduced in isolated perfused working hearts from MHC-ATGL mice, and glucose oxidation was correspondingly enhanced. This was unexpected, since ATGL overexpression was previously shown to increase FAO in the liver *in vivo* and in isolated primary hepatocytes (35, 38, 46) as well as in isolated primary adipocytes (1). Therefore, our data suggest that the effect of ATGL overexpression on FAO is tissue specific. Moreover, the reduction in myocardial FAO also corresponded with decreased mRNA expression of multiple PPARα/δ target genes and PGC1α in MHC-ATGL hearts, suggesting that ATGL overexpression impairs PPARα/δ and PGC1α activities.

In what would appear to be in contrast to our study, a recent study found that ATGL-mediated TG hydrolysis is required for providing the necessary lipid ligands responsible for mediating PPARα/δ activity in the heart (16). Associated with a markedly diminished PPARα/δ target gene and PGC1α/β mRNA expression, ATGL-deficient hearts exhibited severely disrupted mitochondrial oxidation of both glucose and FA, which resulted in energetically and functionally compromised hearts (16). Based on these previous findings, the observed decrease in mRNA expression of multiple PPARα/δ target genes and PGC1α as well as the reduction in FA uptake and oxidation in MHC-ATGL hearts were unexpected. However, our data also suggest that the myocardial TG pool is chronically reduced in MHC-ATGL mice and cannot be expanded during conditions of increased FA supply from the plasma (e.g., fasting). As such, in a manner similar to that in ATGL-deficient hearts (16), the provision of FA from the intramyocardial TG pool is also limited in the ATGL-overexpressing hearts, albeit not to the same extent. Based on this rationale and

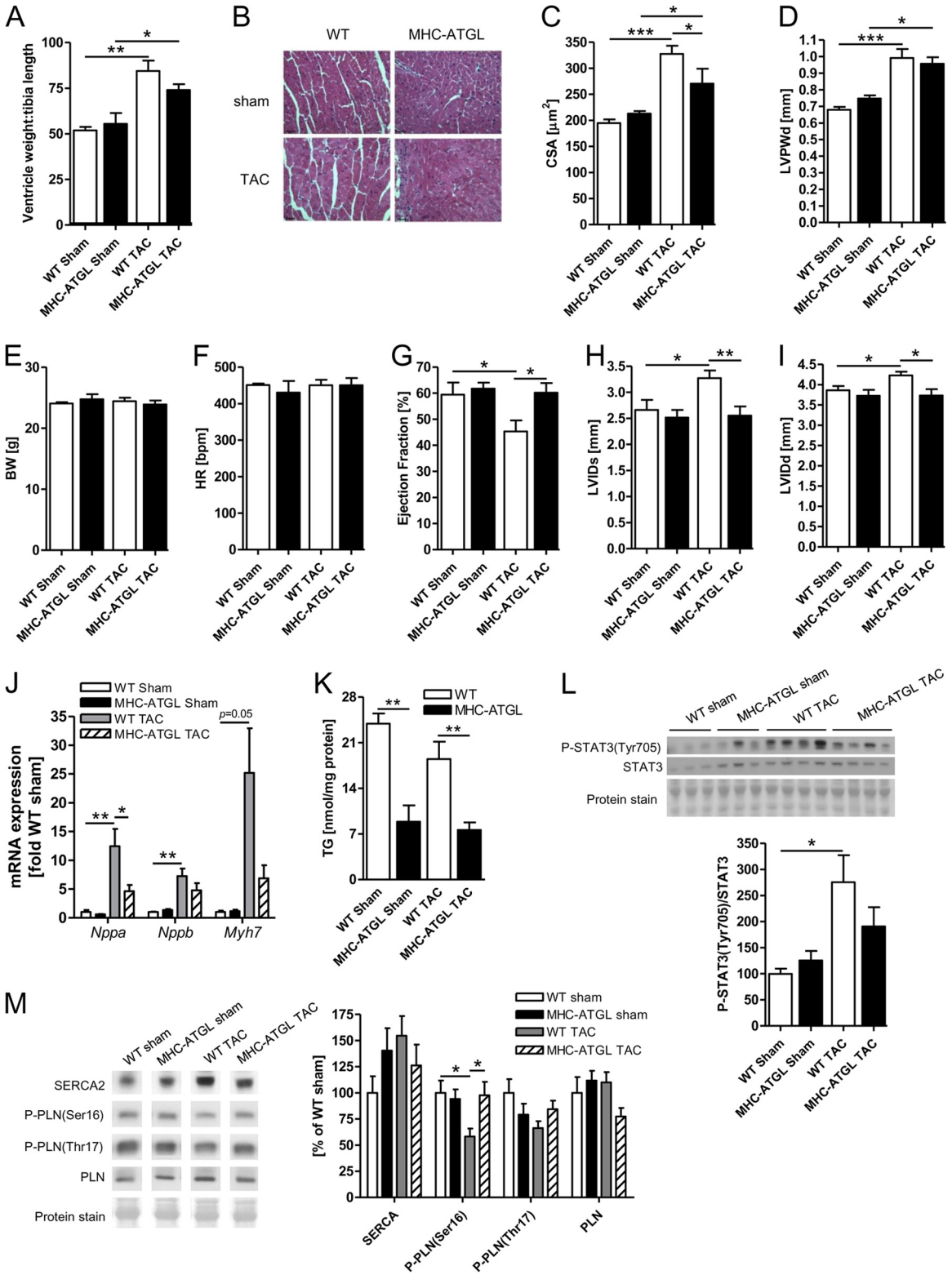

FIG 6 *In vivo* heart function and cardiac morphometry following 5 weeks of TAC. (A) Ratio of ventricle weight to tibia length ($n = 5$ mice for sham, $n = 6$ to 10 mice for TAC; *, $P < 0.05$; **, $P < 0.01$). (B) Representative apical heart sections stained with hematoxylin and eosin visualized at ×400 magnification. Scale bars indicate 30 μm. (C) Cardiomyocyte cross-sectional area of 223 ± 9 myocytes from 4 to 6 mice per group was determined using hematoxylin- and eosin-stained heart sections (*, $P < 0.05$; ***, $P < 0.001$). (D) Left ventricular posterior wall thickness in diastole (LVPWd); (E) body weight; (F) heart rate; (G) ejection fraction; left ventricular internal diameter in systole (LVIDs) (H) and diastole (LVIDd) (I); (J) mRNA expression of hypertrophy marker genes; (K) myocardial TG content; (L) immunoblot analysis of STAT3 phosphorylation (ratio of phosphorylated STAT3 to total STAT3); (M) immunoblot analysis of SERCA2 and phospholamban (PLN) protein expression and PLN phosphorylation (ratio of phosphorylated PLN to total PLN) ($n = 5$ mice for sham, $n = 6$ to 10 mice for TAC; *, $P < 0.05$; **, $P < 0.01$; ***, $P < 0.001$).

our data, we suggest that a chronic reduction in TG content in MHC-ATGL hearts leads to a limited and less flexible supply of FA from intracellular TG stores, which reduces cardiac PPARα/δ activity and PGC1α expression. However, in contrast to the ATGL-deficient hearts (16), there is a compensatory increase in glucose utilization for energy production in MHC-ATGL hearts, and overall Krebs cycle acetyl-CoA production levels as well as ATP contents were similar between WT and MHC-ATGL hearts. Therefore, MHC-ATGL hearts were not energetically compromised and, in fact, were even more efficient since glucose oxidation consumes less O_2 than FAO per amount of ATP produced (29). Based on this, we propose that this increase in cardiac efficiency contributed to the increased workload capacity and baseline systolic function without hypertrophy as well as preservation of cardiac function following TAC in the MHC-ATGL mice. Although we are proposing a metabolic component explaining improved function at baseline, it is also conceivable that cardiac-specific ATGL overexpression alters (lipid) signaling pathways to secondarily influence cardiac function. Given the connection between metabolism of phospholipids and TG (6, 10, 25, 27) and emerging evidence showing that phospholipid metabolism and signaling influence cardiac function (27, 41, 43, 44), it is also possible that altered TG metabolism in MHC-ATGL hearts modulates phospholipid homeostasis to enhance myocardial performance. Future research will help to test these possibilities.

In summary, the data presented herein show for the first time that cardiomyocyte-specific overexpression of a TG hydrolase can moderately improve systolic function in the healthy heart as well as protect the heart from pressure overload-induced cardiac dysfunction. Our findings are consistent with recent studies that have suggested that TG hydrolysis plays a central role in mediating cardiac metabolism and function in both the healthy and the diseased heart (2, 4, 34). As such, we conclude that the regulation of cardiac TG metabolism plays a critical role in cardiac function.

ACKNOWLEDGMENTS

This work was supported by grants from the Canadian Institute of Health Research and the Heart and Stroke Foundation of Canada to J.R.B.D., postdoctoral fellowships from the Heart and Stroke Foundation of Canada and the Canadian Diabetes Association to P.C.K., and an Alberta Innovates-Health Solutions studentship and postdoctoral award to M.M.Y.S. and T.P., respectively, as well as NIH grant R01DK090166 and an HHMI ECA grant to E.E.K.

REFERENCES

1. **Ahmadian M, et al.** 2009. Adipose overexpression of desnutrin promotes fatty acid use and attenuates diet-induced obesity. Diabetes **58**:855–866.
2. **Banke NH, et al.** 2010. Preferential oxidation of triacylglyceride-derived fatty acids in heart is augmented by the nuclear receptor PPARalpha. Circ. Res. **107**:233–241.
3. **Barger PM, Brandt JM, Leone TC, Weinheimer CJ, Kelly DP.** 2000. Deactivation of peroxisome proliferator-activated receptor-alpha during cardiac hypertrophic growth. J. Clin. Invest. **105**:1723–1730.
4. **Birse RT, et al.** 2010. High-fat-diet-induced obesity and heart dysfunction are regulated by the TOR pathway in Drosophila. Cell Metab. **12**:533–544.
5. **Borradaile NM, Schaffer JE.** 2005. Lipotoxicity in the heart. Curr. Hypertens. Rep. **7**:412–417.
6. **Caviglia JM, De Gomez Dumm IN, Coleman RA, Igal RA.** 2004. Phosphatidylcholine deficiency upregulates enzymes of triacylglycerol metabolism in CHO cells. J. Lipid Res. **45**:1500–1509.
7. **Chiu HC, et al.** 2001. A novel mouse model of lipotoxic cardiomyopathy. J. Clin. Invest. **107**:813–822.
8. **Christoffersen C, et al.** 2003. Cardiac lipid accumulation associated with diastolic dysfunction in obese mice. Endocrinology **144**:3483–3490.
9. **Folch J, Lees M, Sloane Stanley GH.** 1957. A simple method for the isolation and purification of total lipides from animal tissues. J. Biol. Chem. **226**:497–509.
10. **Fullerton MD, Hakimuddin F, Bonen A, Bakovic M.** 2009. The development of a metabolic disease phenotype in CTP:phosphoethanolamine cytidylyltransferase-deficient mice. J. Biol. Chem. **284**:25704–25713.
11. **Gao S, et al.** 2007. Leptin activates hypothalamic acetyl-CoA carboxylase to inhibit food intake. Proc. Natl. Acad. Sci. U. S. A. **104**:17358–17363.
12. **Glenn DJ, et al.** 2011. A murine model of isolated cardiac steatosis leads to cardiomyopathy. Hypertension **57**:216–222.
13. **Gulick J, Subramaniam A, Neumann J, Robbins J.** 1991. Isolation and characterization of the mouse cardiac myosin heavy chain genes. J. Biol. Chem. **266**:9180–9185.
14. **Guo D, et al.** 2010. Loss of PI3Kgamma enhances cAMP-dependent MMP remodeling of the myocardial N-cadherin adhesion complexes and extracellular matrix in response to early biomechanical stress. Circ. Res. **107**:1275–1289.
15. **Haemmerle G, et al.** 2006. Defective lipolysis and altered energy metabolism in mice lacking adipose triglyceride lipase. Science **312**:734–737.
16. **Haemmerle G, et al.** 2011. ATGL-mediated fat catabolism regulates cardiac mitochondrial function via PPAR-alpha and PGC-1. Nat. Med. **17**:1076–1085.
17. **Heather LC, et al.** 2006. Fatty acid transporter levels and palmitate oxidation rate correlate with ejection fraction in the infarcted rat heart. Cardiovasc. Res. **72**:430–437.
18. **Hirano K, Ikeda Y, Zaima N, Sakata Y, Matsumiya G.** 2008. Triglyceride deposit cardiomyovasculopathy. N. Engl. J. Med. **359**:2396–2398.
19. **Imahashi K, Mraiche F, Steenbergen C, Murphy E, Fliegel L.** 2007. Overexpression of the Na+/H+ exchanger and ischemia-reperfusion injury in the myocardium. Am. J. Physiol. Heart Circ. Physiol. **292**:H2237–H2247.
20. **Jeppesen J, et al.** 2011. Contraction-induced skeletal muscle FAT/CD36 trafficking and FA uptake is AMPK independent. J. Lipid Res. **52**:699–711.
21. **Kassiri Z, et al.** 2005. Combination of tumor necrosis factor-alpha ablation and matrix metalloproteinase inhibition prevents heart failure after pressure overload in tissue inhibitor of metalloproteinase-3 knock-out mice. Circ. Res. **97**:380–390.
22. **Khan RS, Drosatos K, Goldberg IJ.** 2010. Creating and curing fatty hearts. Curr. Opin. Clin. Nutr. Metab. Care. **13**:145–149.
23. **Kuang M, Febbraio M, Wagg C, Lopaschuk GD, Dyck JR.** 2004. Fatty acid translocase/CD36 deficiency does not energetically or functionally compromise hearts before or after ischemia. Circulation **109**:1550–1557.
24. **Lee Y, et al.** 2004. Hyperleptinemia prevents lipotoxic cardiomyopathy in acyl CoA synthase transgenic mice. Proc. Natl. Acad. Sci. U. S. A. **101**:13624–13629.
25. **Leonardi R, Frank MW, Jackson PD, Rock CO, Jackowski S.** 2009. Elimination of the CDP-ethanolamine pathway disrupts hepatic lipid homeostasis. J. Biol. Chem. **284**:27077–27089.
26. **Lerch R, Tamm C, Papageorgiou I, Benzi RH.** 1992. Myocardial fatty acid oxidation during ischemia and reperfusion. Mol. Cell. Biochem. **116**:103–109.
27. **Lim HY, Wang W, Wessells RJ, Ocorr K, Bodmer R.** 2011. Phospholipid homeostasis regulates lipid metabolism and cardiac function through SREBP signaling in Drosophila. Genes Dev. **25**:189–200.
28. **Liu L, et al.** 2009. DGAT1 expression increases heart triglyceride content but ameliorates lipotoxicity. J. Biol. Chem. **284**:36312–36323.
29. **Lopaschuk GD, Ussher JR, Folmes CD, Jaswal JS, Stanley WC.** 2010. Myocardial fatty acid metabolism in health and disease. Physiol. Rev. **90**:207–258.
30. **Luiken JJ, Willems J, van der Vusse GJ, Glatz JF.** 2001. Electrostimulation enhances FAT/CD36-mediated long-chain fatty acid uptake by isolated rat cardiac myocytes. Am. J. Physiol. Endocrinol. Metab. **281**:E704–E712.
31. **Marfella R, et al.** 2009. Myocardial lipid accumulation in patients with pressure-overloaded heart and metabolic syndrome. J. Lipid Res. **50**:2314–2323.
32. **McGavock JM, Victor RG, Unger RH, Szczepaniak LS.** 2006. Adiposity of the heart, revisited. Ann. Intern. Med. **144**:517–524.
33. **Ng AC, et al.** 2010. Myocardial steatosis and biventricular strain and strain rate imaging in patients with type 2 diabetes mellitus. Circulation **122**:2538–2544.

34. **O'Donnell JM, Fields AD, Sorokina N, Lewandowski ED.** 2008. The absence of endogenous lipid oxidation in early stage heart failure exposes limits in lipid storage and turnover. J. Mol. Cell. Cardiol. **44**:315–322.
35. **Ong KT, Mashek MT, Bu SY, Greenberg AS, Mashek DG.** 2011. Adipose triglyceride lipase is a major hepatic lipase that regulates triacylglycerol turnover and fatty acid signaling and partitioning. Hepatology **53**:116–126.
36. **Oudit GY, et al.** 2008. Loss of PTEN attenuates the development of pathological hypertrophy and heart failure in response to biomechanical stress. Cardiovasc. Res. **78**:505–514.
37. **Preiss J, et al.** 1986. Quantitative measurement of sn-1,2-diacylglycerols present in platelets, hepatocytes, and ras- and sis-transformed normal rat kidney cells. J. Biol. Chem. **261**:8597–8600.
38. **Reid BN, et al.** 2008. Hepatic overexpression of hormone-sensitive lipase and adipose triglyceride lipase promotes fatty acid oxidation, stimulates direct release of free fatty acids, and ameliorates steatosis. J. Biol. Chem. **283**:13087–13099.
39. **Saddik M, Lopaschuk GD.** 1991. Myocardial triglyceride turnover and contribution to energy substrate utilization in isolated working rat hearts. J. Biol. Chem. **266**:8162–8170.
40. **Schweiger M, Lass A, Zimmermann R, Eichmann TO, Zechner R.** 2009. Neutral lipid storage disease: genetic disorders caused by mutations in adipose triglyceride lipase/PNPLA2 or CGI-58/ABHD5. Am. J. Physiol. Endocrinol. Metab. **297**:E289–E296.
41. **Sentex E, Sergiel JP, Lucien A, and Grynberg A.** 1998. Is the cytoprotective effect of trimetazidine associated with lipid metabolism? Am. J. Cardiol. **82**:18K–24K.
42. **Son NH, et al.** 2010. PPARgamma-induced cardiolipotoxicity in mice is ameliorated by PPARalpha deficiency despite increases in fatty acid oxidation. J. Clin. Invest. **120**:3443–3454.
43. **Tabbi-Anneni I, et al.** 2003. Prevention of heart failure in rats by trimetazidine treatment: a consequence of accelerated phospholipid turnover? J. Pharmacol. Exp. Ther. **304**:1003–1009.
44. **Tappia PS, Singal T.** 2008. Phospholipid-mediated signaling and heart disease. Subcell. Biochem. **49**:299–324.
45. **Tsai JY, et al.** 2010. Direct regulation of myocardial triglyceride metabolism by the cardiomyocyte circadian clock. J. Biol. Chem. **285**:2918–2929.
46. **Turpin SM, et al.** 2011. Adipose triacylglycerol lipase is a major regulator of hepatic lipid metabolism but not insulin sensitivity in mice. Diabetologia **54**:146–156.
47. **Ussher JR, et al.** 2009. Insulin-stimulated cardiac glucose oxidation is increased in high-fat-diet-induced obese mice lacking malonyl CoA decarboxylase. Diabetes **58**:1766–1775.
48. **Zimmermann R, et al.** 2004. Fat mobilization in adipose tissue is promoted by adipose triglyceride lipase. Science **306**:1383–1386 .